ARMA 14-6949

Micro-Macro Modeling Approach for the Triggering of Viscous Fatigue Damage in Halite Polycrystals under Cyclic Loading

Pouya, A.
Laboratoire Navier (ENPC/IFSTTAR/CNRS), Ecole des Ponts Paris Tech, Champs sur Marne, France
Zhu, C. and Arson, C.
Geosystems group, School of Civil and Environmental Engineering,
Georgia Institute of Technology, Atlanta, Georgia, USA.

ABSTRACT: Underground cavities in salt rock formations used for Compressed Air Energy Storage (CAES) undergo cyclic loads and are subject to a fatigue phenomenon that induces a decrease of rock's strength and stiffness. A micromechanical analysis of this phenomenon is necessary to understand its mechanisms and elaborate relevant constitutive models. The polycrystalline nature of rock salt has a crucial effect on crack propagation and rock damage and, hence, on fatigue behavior. This behavior was investigated herein on the basis of self consistent upscaling approaches for viscous heterogeneous materials. The internal stresses in the polycrystal were modeled based on experimental data available for halite single crystals, and a monotonic compression test was simulated, which allowed tracking the triggering of fatigue damage. Results show that tensile stresses are developed in the polycrystal under global compressive load, the amplitude of which depends on the macroscopic load rate or frequency. These tensile stresses can exceed in some conditions the tensile strength of grains or of grains interfaces and cause cracking and damage in the polycrystal.

1. INTRODUCTION

Salt cavities used for the underground storage of oil and natural gas undergo weekly to seasonal thermo-mechanical load cycles. Compressed Air Energy Storage (CAES) facilities are subject to shorter load cycles, of the order of a day. Experimental data shows that the resulting fatigue of salt rock (i.e., decrease of Young's modulus and strength) decreases as the load frequency increases. Fatigue is an important dimensioning factor for CAES design. However, due to the numerous variables influencing salt damage under cyclic loading (e.g., stress amplitude, loading frequency), and due to the high number of cycles necessary to assess fatigue effects in the laboratory, experimental characterization of fatigue in salt rock remains a challenge.

In the present paper, an attempt is made to analyze the origin of salt fatigue from the study of deformation micro-mechanisms, i.e. from the mechanisms driving the deformation of halite crystals in the polycrystalline material. Plastic and viscous deformation of salt crystals result from several fundamental mechanisms, e.g., dislocation glide, dislocation climb, polygonalization, inter-granular slip, dissolution-precipitation. Under stress and temperature typical of storage conditions, dislocations are the predominant mechanisms contributing to macroscopic salt rock deformation. Dislocation movements can only occur on specific crystallographic surfaces, and in a limited number of directions. Restricted movements inside a monocrystalline grain cause incompatibilities between non-elastic deformations of adjacent grains, which results into internal stresses within the polycrystal. In this paper, it is proposed to model the macroscopic viscous behavior of the polycrystalline medium with the self-consistent method.

The upscaling approach is explained in Section 2. Following the approach adopted in [1, 2, 3] to model salt rock plastic behavior, a microscopic viscous sliding model is formulated at the crystal scale in Section 3. Section 4 presents a computational method to calculate internal stresses in the polycrystal during cyclic loading and to deduce the crack initiation and fatigue of the polycrystal. A monotonic uniaxial compression test is simulated to illustrate how the model can capture the triggering of fatigue. Results are presented in Section 5.

2. MULTISCALE MODELING APPROACH

2.1. The Self-Consistent Method

In upscaling methods, the macroscopic behaviour of a heterogeneous material is deduced from the relations between the averages stress and strain values in the materials constituents. The strain and strain in a constituent, modeled as a grain in an aggregate, are determined by macroscopic load on the aggregate and the interaction between different grains. This interaction is usually simplified and represented by a so-called inclusion-matrix model": an inclusion representing the grain is embedded in an infinite homogeneous matrix that represents the aggregate behaviour at macroscopic scale. Since the matrix behaviour is a priori unknown, this upscaling method leads to an implicit system of equations. The unknown matrix model has to be determined iteratively, so as to relate average strains and stresses in the grains. This procedure is called the self-consistent upscaling scheme. In this method the inclusion-matrix interaction model plays a central role. The balance of microscopic stresses at the boundaries between two constituents is ensured by correcting the macroscopic stress (resp. strain) field by a so-called eigenstress (resp. eigenstrain) field. REV properties (such as the REV stiffness matrix) are deduced from the knowledge of stress (resp. strain) concentration tensors, which depend on the geometry of the heterogeneity present in the REV [4, 5].

2.2. Inclusion Matrix Model

Salt Rock is made of halite (NaCl) monocrystals (also called “grains”), which have all the same FCC (Face-Centered Cubic) structure and atomic composition. Monocrystals are randomly oriented. In the proposed model, it is assumed that all possible grain orientations have the same probability of occurrence, i.e. monocrystal orientation (Ω) follows a uniform probability density function (p_ω). Considering for instance 200 equally-spaced points on a sphere, each of which characterized by a solid angle Ω_k:

$$\forall k = 1,2,\dots,200,\ p_\omega(\Omega_k) = \frac{1}{200} \tag{1}$$

The Representative Elementary Volume (REV) is defined as the minimum volume containing the 200 possible grain orientations considered in the model. The average of a function f is defined as:

$$\begin{aligned} \bar{f}(x) = < f(x) > &= \int_\Omega p_\omega(\omega) f(x,\omega) d\omega \\ &= \frac{1}{200}\sum_{k=1}^{200} f(x,\Omega_k) \end{aligned} \tag{2}$$

The self-consistent method is employed to relate the microscopic stress developing in a monocrystal to the macroscopic stress applied in the far field (at the boundary of the REV): the grains surrounding the monocrystal under study are viewed as a homogeneous matrix, and the monocrystal is modeled as an inclusion in that matrix. Figure 1 illustrates the principle of the inclusion-matrix model followed in this study, and explains the notations adopted for the local (grain-scale) and global (REV-scale) coordinate systems.

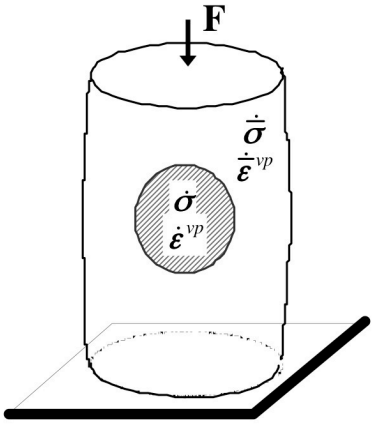

Fig. 1. Schematic representation of salt crystals.

Both monocrystals and the matrix are assumed to be viscoplastic. Weng’s viscoelastic self-consistent model [6] is based on the Eshelby's inclusion model, and assumes that the matrix-inclusion interaction can be captured with a purely elastic matrix behaviour model (i.e. macroscopic viscoplasticity only stems from grain-scale viscoplastic deformation, and not from grain/matrix incompatibilities). The local stress (in the grain inclusion) and far field stress (in the matrix) are coupled to viscous strain rates by the same relationship as in Kröner model (which holds for elastic-plastic materials):

$$\dot{\boldsymbol{\sigma}} = \dot{\bar{\boldsymbol{\sigma}}} + 2\mu(1-\beta)(\dot{\bar{\boldsymbol{\epsilon}}}^{\boldsymbol{vp}} - \dot{\boldsymbol{\epsilon}}^{\boldsymbol{vp}}) \tag{3}$$

Where β is given by:

$$\beta = \frac{2(4-5\nu)}{15(1-\nu)} \tag{4}$$

In which ν is the Poisson's ratio of the homogenized REV (a priori unknown). It is worth noting this model has been criticized later by [7] who pointed out that, because Kröner model is not self-consistent for elastic-plastic materials, Weng’s model is not really self-consistent for viscoplastic materials either. Indeed Weng model does not take into account the viscous interaction between the inclusion and the matrix. However, it constitutes a very simple approximation of the real interaction model and is sufficient for the purposes of this paper, which focuses on macroscopic fatigue behavior induced by cyclic loading.

3. GRAIN-SCALE CONSTITUTIVE MODEL

3.1. Halite Crystalline Structure and Sliding Mechanisms

Halite is a cluster of perfect Face-Centered Cubic crystals (FCC). If all constituents of the crystal were atoms, intra-granular dislocations would occur on planes separating the two densest grain fractions, i.e. on planes normal to the <111> direction of the grain coordinate system. However, halite crystals comprise two FCC ionic sub-networks (sodium Na^+ and chloride Cl^-) (Fig. 2).

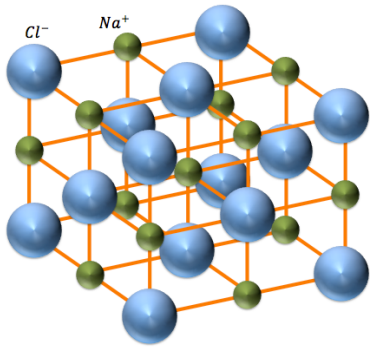

Fig. 2. Face-Centered Cubic (FCC) crystal structure of salt.

Due to electronic interaction forces between ions, preferential sliding planes (i.e. planes along which sliding requires the minimum energy input) are the {101} planes, i.e. the six planes normal to directions:

$$\boldsymbol{N^1}=\frac{1}{\sqrt{2}}\begin{Bmatrix}0\\1\\1\end{Bmatrix}\quad \boldsymbol{N^2}=\frac{1}{\sqrt{2}}\begin{Bmatrix}1\\0\\1\end{Bmatrix}\quad \boldsymbol{N^3}=\frac{1}{\sqrt{2}}\begin{Bmatrix}-1\\-1\\0\end{Bmatrix}$$
$$\boldsymbol{N^4}=\frac{1}{\sqrt{2}}\begin{Bmatrix}0\\-1\\1\end{Bmatrix}\quad \boldsymbol{N^5}=\frac{1}{\sqrt{2}}\begin{Bmatrix}-1\\0\\1\end{Bmatrix}\quad \boldsymbol{N^6}=\frac{1}{\sqrt{2}}\begin{Bmatrix}-1\\1\\0\end{Bmatrix} \tag{5}$$

In which the sliding directions are respectively:

$$\boldsymbol{M^1}=-\boldsymbol{N^4}\quad \boldsymbol{M^2}=-\boldsymbol{N^5}\quad \boldsymbol{M^3}=-\boldsymbol{N^6}$$
$$\boldsymbol{M^4}=-\boldsymbol{N^1}\quad \boldsymbol{M^5}=-\boldsymbol{N^2}\quad \boldsymbol{M^6}=-\boldsymbol{N^3} \tag{6}$$

Sliding system $\boldsymbol{N^4}\otimes\boldsymbol{M^4}$ (resp. $\boldsymbol{N^5}\otimes\boldsymbol{M^5}$ and $\boldsymbol{N^6}\otimes\boldsymbol{M^6}$) is normal to sliding system $\boldsymbol{N^1}\otimes\boldsymbol{M^1}$ (resp. $\boldsymbol{N^2}\otimes\boldsymbol{M^2}$ and $\boldsymbol{N^4}\otimes\boldsymbol{M^4}$). Moreover:

$$\boldsymbol{N^1}\otimes\boldsymbol{M^1}=\boldsymbol{N^2}\otimes\boldsymbol{M^2}+\boldsymbol{N^3}\otimes\boldsymbol{M^3} \tag{7}$$

So there are only two independent sliding mechanisms for each grain. Note: sliding systems noted $\boldsymbol{A^l}=\boldsymbol{N^l}\otimes\boldsymbol{M^l}$ are expressed in the coordinate systems attached to the grain. Grains can take different orientations in the REV. Considering 200 possible grain orientations, there are $6\times200=1{,}200$ possible sliding mechanisms in the REV, among which only 400 are independent.

3.2. Grain-Scale Viscoplastic Model

The sliding system of the grain (i.e. mono-crystal), expressed in global matrix coordinates, is noted:

$$a_{ij}^{l}=\frac{n_i m_j+n_j m_i}{2} \tag{8}$$

In which $\boldsymbol{n}$ and $\boldsymbol{m}$ are respectively the vector normal to the sliding plane and the unit sliding vector. The viscoplastic deformation of the grain writes:

$$\dot{\epsilon}_{ij}^{vp}=\sum_{l=1}^{L}\dot{\gamma}^{l}a_{ij}^{l} \tag{9}$$

In which $\dot{\gamma}^l$ is the viscoplastic (shear) deformation of grains subjected to the sliding mechanism in the grain. L is the total number of active sliding mechanisms. For halite mono-crystals, with only 2 independent sliding mechanisms). Noting $\boldsymbol{\tau^l}=\boldsymbol{\sigma}:\boldsymbol{a^l}$, we assume that the irreversible shear deformation obeys a power law:

$$\dot{\gamma}^{l}=\left(\frac{\tau^{l}}{\tau_0}\right)^{n} \tag{10}$$

In which n and τ_0 are two material constants, which can be obtained from [8], considering only 4 active slip systems at room temperature.

4. REV-SCALE DAMAGE INITIATION

4.1. Expression of Micro-stress in One Grain (Monocrystal)

A method is proposed to compute micro-stresses in a REV subjected to far field cyclic axial loading. We note:

$$\bar{\boldsymbol{\sigma}}=q(t)\boldsymbol{r},\ \bar{s}=\bar{\boldsymbol{\sigma}}-\frac{tr(\bar{\sigma})}{3}\boldsymbol{\delta}=q(t)\boldsymbol{\Psi},\ \dot{\bar{\boldsymbol{\epsilon}}}^{vp}=\frac{3}{2}\dot{p}(t)\boldsymbol{\Psi} \tag{11}$$

In which:

$$[\boldsymbol{r}]=\begin{bmatrix}0&0&0\\0&0&0\\0&0&-1\end{bmatrix}\quad[\boldsymbol{\Psi}]=\begin{bmatrix}1/3&0&0\\0&1/3&0\\0&0&-2/3\end{bmatrix} \tag{12}$$

According to Eq. (9), the microscopic and macroscopic viscoplastic strains are purely deviatoric. Taking the deviatoric part of Eq. (3) thus yields:

$$\dot{\boldsymbol{s}}=\dot{\bar{\boldsymbol{s}}}+2\mu(1-\beta)(\dot{\bar{\boldsymbol{\epsilon}}}^{vp}-\dot{\boldsymbol{\epsilon}}^{vp}) \tag{13}$$

Factorizing by operator $[\Psi]$:

$$\dot{\boldsymbol{s}}=\dot{\rho}(t)\boldsymbol{\Psi}-2\mu(1-\beta)\dot{\boldsymbol{\epsilon}}^{vp} \tag{14}$$

Where

$$\dot{\rho}(t)=\dot{q}(t)+3\mu(1-\beta)\dot{p}(t) \tag{15}$$

In Eq. (14) above, $\dot{\epsilon}^{vp}$ depends on sliding systems expressed in global coordinates. The l^{th} sliding mechanisms of the grain in the p^{th} global coordinate system ($\boldsymbol{a^{l,p}}$) are obtained from the sliding mechanisms expressed in the local coordinate system of the grain ($\boldsymbol{A^l}$):

$$[\boldsymbol{a^{l,p}}]=[\boldsymbol{P^p}][\boldsymbol{A^l}][\boldsymbol{P^p}]^T \tag{16}$$

Where $[\boldsymbol{P}]=[\boldsymbol{P_1}][\boldsymbol{P_2}][\boldsymbol{P_3}]$. Noting Ψ^p, θ^p and Φ^p are three spherical coordinates of grain in the 3D space (dropping the index for clarity):

$$[\boldsymbol{P_1}]=\begin{bmatrix}cos\Psi&sin\Psi&0\\-sin\Psi&cos\Psi&0\\0&0&1\end{bmatrix} \tag{17}$$

$$[\boldsymbol{P_2}] = \begin{bmatrix} cos\theta & 0 & sin\theta \\ 0 & 1 & 0 \\ -sin\theta & 0 & cos\theta \end{bmatrix}$$

$$[\boldsymbol{P_3}] = \begin{bmatrix} cos\Phi & -sin\Phi & 0 \\ sin\Phi & cos\Phi & 0 \\ 0 & 0 & 1 \end{bmatrix}$$

4.2. Micro-macro Viscoplastic Law

Taking the mean of the expression in Eq. (14):

$$\dot{\bar{\boldsymbol{s}}} = \dot{\rho}(t)\boldsymbol{\Psi} - 2\mu(1-\beta) < \dot{\boldsymbol{\epsilon}}^{\boldsymbol{vp}} > \quad (18)$$

Substituting macroscopic stress and microscopic viscoplastic strain by their values:

$$\dot{q}(t)\boldsymbol{\Psi} = \dot{\rho}(t)\boldsymbol{\Psi} - 2\mu(1-\beta) < \sum_{l=1}^{L} \left(\frac{q(t)\boldsymbol{r}:\boldsymbol{a^l}}{\tau_0} \right)^n \boldsymbol{a^l} > \quad (19)$$

Dividing both sides by $\boldsymbol{\Psi}$ and make some rearrangements, Eq. (19) can be simplified into:

$$\dot{q}(t) = \dot{\rho}(t) - q^n(t) \underbrace{\frac{3\mu(1-\beta)}{(\tau_0)^n} < \sum_{l=1}^{L} \left(\boldsymbol{r}:\boldsymbol{a^l}\right)^{n+1} >}_{A} \quad (20)$$

The expression of q as a function of time is obtained by solving the following non-linear differential equation:

$$\dot{q}(t) + Aq^n(t) = \dot{\rho}(t) \quad (21)$$

Combining with Eq. (15), the following equation that relates $\dot{q}(t)$ and $\dot{p}(t)$ through A, is obtained as:

$$\dot{p}(t) = \frac{A}{3\mu(1-\beta)} q^n(t) \quad (22)$$

The exact expression of A depends on an integral of trigonometric functions on all the possible values of the solid angle in a 3D space. In the expression for A (Eq. (20)), this integral is discretized in the form of a sum, for 200 uniformly distributed crystal orientations. The macroscopic viscoplastic law can easily be deduced from Eq. (22):

$$\dot{\bar{\epsilon}}^{vp} = \frac{3}{2} \frac{< \sum_{l=1}^{L} \left(\boldsymbol{r}:\boldsymbol{a^l}\right)^{n+1} >}{(\tau_0)^n} q^n(t)\Psi \quad (23)$$

4.3. Damage Initiation

Damage at the REV scale triggers when one mono-crystal fails, i.e. when microstress in a grain reaches the compression strength or the tension strength of the mono crystal. Fracture at the grain scale occurs first in mono-crystals subject to the highest microstress. Macroscopic damage initiates if microstress exceeds grain compression strength or tension strength for at least one mono-crystal orientation. The following developments aim to express microstress as a function of the orientation of the mono-crystal, in order to detect the triggering of damage at the REV scale. From Equations 3 and 11:

$$\dot{\boldsymbol{\sigma}} = \dot{q}(t)\boldsymbol{r} + 2\mu(1-\beta)\left(\frac{3}{2}\dot{p}(t)\boldsymbol{\Psi} - \dot{\boldsymbol{\epsilon}}^{\boldsymbol{vp}}\right) \quad (24)$$

As a result, for any grain, microscopic stress is related to the directions of the sliding mechanisms according to the following equation:

$$\dot{\boldsymbol{\sigma}} = \dot{q}(t)\boldsymbol{r} + Aq^n(t)\boldsymbol{\Psi} - 2\mu(1-\beta)\sum_{l=1}^{L} \dot{\gamma}^l \boldsymbol{a^l} \quad (25)$$

In which $\boldsymbol{a^l} = \boldsymbol{a^{l,p}}$ (for the current grain) is related to the orientation of the mono crystal according to Eq. (16). Assuming that the test is stress-controlled (i.e., $q(t)$ is known at any time), it is possible to determine the grain orientations (characterized by the three angles Ψ^p, θ^p, Φ^p) that maximize $\dot{\boldsymbol{\sigma}}$.

5. NUMERICAL ANALYSIS

5.1. Problem Statement

A numerical program was developed in MATLAB for the calculation of the polycrystalline behavior at the REV scale based on the model framework presented above. A stress-controlled uniaxial compression test was simulated. The average quantities were calculated on 200 grains of different directions. The imposed macroscopic stress followed a sinusoidal function:

$$q(t) = q_0 sin\,(\omega t), \quad \dot{q}(t) = q_0 \omega cos(\omega t) \quad (26)$$

Only one quarter of the period was simulated, which allowed studying the triggering of fatigue damage under monotonic loading while considering the frequency dependency. Three cases with the same maximum loading but three loading frequencies (1×10^{-5} Hz, 2×10^{-5} Hz, and 3×10^{-5} Hz) were analyzed. Input parameters for the simulation are summarized in Table 1.

Table 1. Model parameters used for the simulation of stress-controlled uniaxial compression.

E (MPa)	ν (-)	L (-)
25000	0.25	4
q_0 (MPa)	τ_0 (MPa)	n (-)
45	55	15

5.2. Evolution of Macro-stress and Macro-strain

Time evolutions of macroscopic loading are different in the three cases, as illustrated in Figure 3. For higher frequency, the peaking loading is reached within a shorter time (Fig. 3a). Therefore, at the same moment, larger macro-stress is obtained if the frequency is higher.

The macroscopic stress-strain curve follows the expected trends (Fig. 3b). Since this is a viscoplastic model, all slip mechanisms are active. There is no slip before the stress reaches certain level. The stiffness increases with

frequency because the viscous behavior has less time to be produced at higher frequency.

The amplitude of macroscopic strain obtained with loading at higher frequency is smaller (Fig. 3c). This is also a consequence of less viscous behavior and less slip under higher frequency. However, the strain level that can be reached at the maximum loading is smaller than that observed in experiments performed on salt rock [8]. Indeed the model applies for perfect polycrystals with no cracks or impurities, which can increase strains in real rocks.

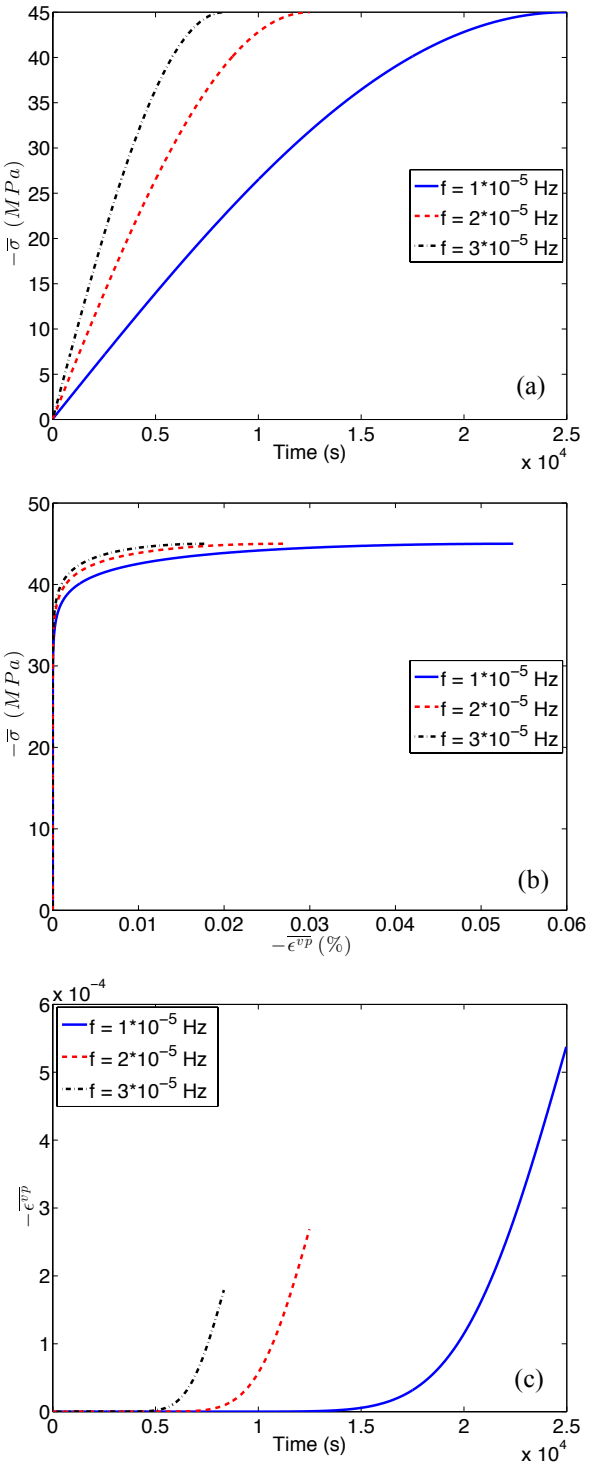

Fig. 3. Stress and strain evolution at macroscopic level.

5.3. *Distribution of Micro-stress*

For the case of a uniaxial compression loading, due to the axial symmetry condition around the compression axis $\vec{z}$, the local stress distribution in the polycrystal can be represented graphically.

The vector $\sigma_i \vec{v}$ can be used to represent a principal stress, where the unit vector $\vec{v}$ represents the principal direction and σ_i is the magnitude of the principal stress. A vector in the radial plane is used to indicate the principal stress of the grain (Fig. 4). Due to the axisymmetric condition, principal direction can be plotted in the first quadrant (r>0, z>0). If the principal stress is positive (tensile stress), the point will be placed in the same quadrant, and if negative (compressive stress), the point will be located in the opposite quadrant. Therefore, given the vector in the stress map, the orientation, the amplitude, and the sign of the principal stress can be obtained.

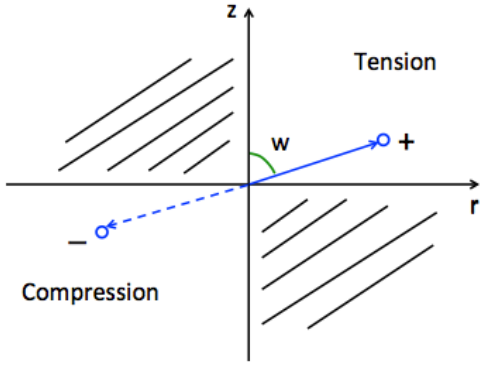

Fig. 4. Representation of local principal stress [1].

Figure 5a represents the distribution diagram for the major and minor stresses of each grain. Each point of the upper group (triangular mark) represents the major principal stress of one of the 200 grains constituting the polycrystal. For most grains, the major stress is a tensile stress radially distributed in the 1st quadrant with a small angle with the r-axis. This implies that cracks are parallel to the compression axis, which is usually observed in laboratory tests. For some grains, the amplitude of the major principal micro-stress exceeds the tensile strength of salt (about 2 MPa).

The microscopic stress between grains decreases with increased frequency. This is a result of incompatibility (heterogeneity) of the viscous strain of grains, which decreases with frequency.

Comparing the results in the local stress distribution plot for three different loading frequencies, it can be observed that for lower frequency (longer period), the tensile micro-stress magnitude increases, which leads to a higher probability of grain failure. In Figure 5b, when the frequency is increased, the tensile stress drops to below 2 MPa, which suggests that the failure of the

polycrystalline is most likely to occur in the lower frequency case.

Research work has been undertaken needed to understand the variations of compressive microscopic stress with frequency in stress-controlled tests, and to minimize the numerical errors that can occur when very low strains need to be computed.

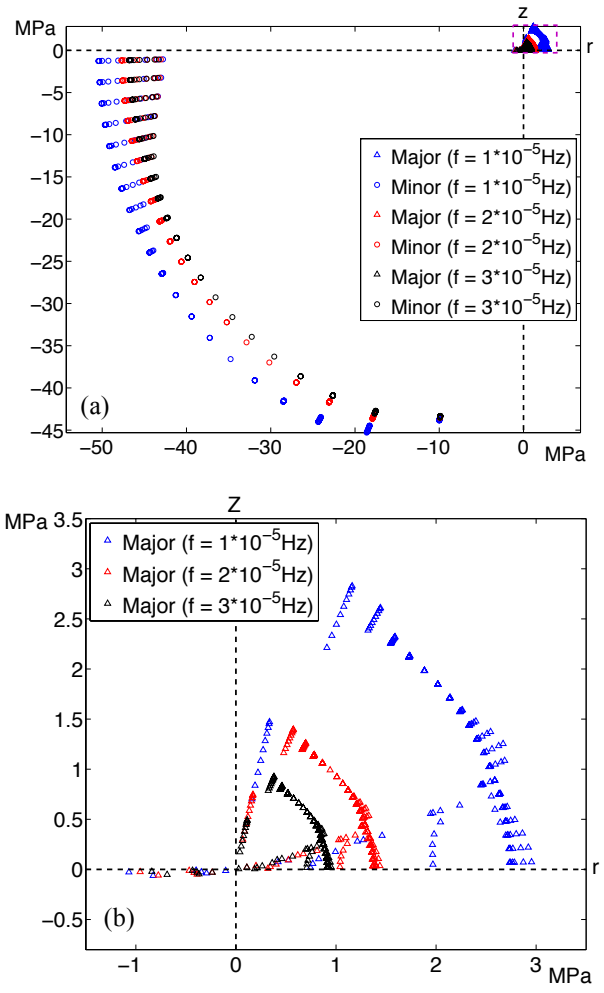

Fig. 5. Orientation and intensity of micro-stress in the grains.

6. CONCLUSION

The micromechanical modeling approach adopted herein allows predicting the triggering of fatigue damage due to microstress accumulation in polycrystalline rock salt under cyclic loading. The model captures the dependency of the damage threshold to the load frequency and amplitude.

Fatigue is simulated at the REV scale of polycrystalline salt subjected to stress-controlled uniaxial compression loading. Macro-stress increases with the loading frequency whereas maximum macro-strain decreases with the frequency.

Tensile micro-stress developed in the polycrystal is perpendicular to the macro-compression direction. Tensile micro-stress amplitude increases with larger macro-stress and lower loading frequency. Numerical results verify that strength limits are less likely to be exceeded under high load frequencies, which is in agreement with laboratory observation.

The proposed micro-macro approach opens an interesting way to study the rock salt fatigue, which is an important issue for the design and conception of underground storage cavities in rock salt.

REFERENCES

1. Pouya, A. 1991. *Comportement rhélogique du sel gemme. application l'érude des excavations souterraines.* Ph.D. thesis. Ecole Nationale des Ponts et Chaussées, Paris.
2. Pouya, A. 1991. Correlation between mechanical behaviour and petrological properties of rock salt. In *Proceedings of the 32nd US Symposium on Rock Mechanics (USRMS)*, 1991, pp. 385-392.
3. Pouya, A. 2000. Micromacro approach for the rock salt behavior. *Eur. J. Mech. A/Solids* 19: 1015-1028.
4. Nemat-Nasser, S. and M. Hori. Micromechanics: overall properties of heterogeneous solids. *Applied Mathematics and Mechanics.* Elsevier, Amsterdam.
5. Berryman, J. G. 1995. Mixture theories for rock properties. In *Rock Physics & Phase Relations: A Handbook of Physical Constants.* 205-228.
6. Weng, G. 1982. A unified self-consistent theory for the plastic-creep deformation of metals. *J. Appl. Mech.* 49: 728-734.
7. Rougier, Y., C. Stolz, and A. Zaoui. 1994. Self-consistent modeling of elastic-viscoplastic polycrystals. *C.R. Acad. Sci. Paris*. série II 318: 145-151.
8. Wanten, P.H., C.J. Spiers, and C.J. Peach. 1993. Deformation of NaCl single crystals. In *3rd Conference on the Mechanical Behavior of Salt*. Ecole Polytechnique, Palaiseau, France.